Journal of Molecular Structure 1291 (2023) 135890

Contents lists available at ScienceDirect

Journal of Molecular Structure

journal homepage: www.elsevier.com/locate/molstr

Ionic, charge transfer interactions, reactivity of the NLO molecule morpholinium perchlorate comparison with morpholinium derivatives using DFT method

C.L. Shiny [a,1], A. Arun Kumar [b,1], C. Dabora Vincy [c,1], X.D. Divya Dexlin [a,1], J.D. Deephlin Tarika [a,1], T. Joselin Beaula [a,1,*]

[a] Department of Physics and Research Centre, Malankara Catholic College, Mariagiri 629153, Tamilnadu, India
[b] Department of Physics (H&Sc), Methodist College of Engineering & Technology (Autonomous), Abids, Hyderabad 500001, India
[c] Department of Physics, Marudhar Kesari Jain College for Women, Vaniyambadi 635751, India

ARTICLE INFO

Keywords:
Ionic interactions
Density overlap region indicator analysis
NLO effects

ABSTRACT

In the present study, the compound morpholinium perchlorate (MP) was explored using spectroscopic methods and quantum chemical computations. A TD-DFT method was employed to study the charge transfer ionic interaction strategy to identify the electronic transition exhibited in the UV–visible spectrum, and vibrational analysis of FT-IR and FT-Raman was also measured experimentally. Natural population analysis and molecular electrostatic potential (MEP) surface analysis of the molecule were performed to predict the molecule's reactive site. Natural bond orbital analysis (NBO) and natural charge analysis were used to study the charge transfer interaction. The nature of inter and intramolecular hydrogen bonds are analyzed by using reduced density gradient (RDG), density overlap region indicator (DORI) analysis, and Hirshfeld surface analysis. Electron localization function (ELF) and analysis provide new insight into the chemical bonding of MP. The NLO activity of the studied compound was highlighted by computing the first and second order hyperpolarizability. In the current investigation, the effects of MP and a few morpholinium derivatives were contrasted in terms of molecular geometry, vibrational assessment, HOMO-LUMO energy gap, and NLO effects. According to the results, the MP can be effectively used as an optical limiter in optoelectronics.

1. Introduction

A colorless, oily, volatile organic chemical molecule called morpholin is a good nucleophile because its six-membered ring exposes the single electron pair on nitrogen [1]. Morpholinium-based compounds offer intriguing physiochemical characteristics, significant electrochemical features, high ionic conductivity, low cost, and low toxicity, making them particularly advantageous for use as an electrolyte in batteries and capacitors [2,3]. However, because of their low toxicity, morpholinium cations are recommended and employed as green solvents, particularly in the industrial sector [4]. Due to single crystals' significance for both fundamental and practical research, the development of single crystals and their characterization for device manufacture have gained significant momentum. Metal-organic compounds stand out among nonlinear optical (NLO) crystals. In the realm of solid-state electronics, these crystals are becoming more and more significant [1]. The prevalence of the optical sector prompted to study of the optical activity of the compound which is reported in the present study. Molecular properties, DFT calculations of morpholinium tetra chloropalladate (II) (MTCP) has reported by Umadevi et al. [5]. Bhuvaneswari et al. have reported the molecular structure, vibrational spectroscopic (FT-IR, FT-Raman), NBO, HOMO and LUMO analyses of morpholinium oxalate (MO) by DFT method [6]. Crystal structure and database study of quaternary phosphoniumcation and perchlorate anions coordination reported by Salmasi et al. [7]. Arunkumar et al. reported the structure and few experimental details of the Morpholinium Perchlorate (MP) compound [8].

A comprehensive assessment of the literature has revealed that there's been no substantial theoretical quantum chemical research on the specified compound Morpholinium Perchlorate molecule to date.

* Corresponding author.
E-mail address: joselinbeaula@gmail.com (T.J. Beaula).
[1] Affiliated to Manonmaniam Sundaranar University, Abishekapatti-627012, Tirunelveli, Tamilnadu, India.

https://doi.org/10.1016/j.molstruc.2023.135890
Received 14 November 2022; Received in revised form 20 May 2023; Accepted 28 May 2023
Available online 29 May 2023

Today, experimental techniques are no longer enough to completely characterize a complex molecular structure and the best way is to combine the experimental with theoretical methods. Computational methods can be an important tool to increase the accuracy of the characterization process and report some key physicochemical properties. The NLO property and other molecular characteristics of the MP molecule were examined and compared to those of related substances such as, morpholinium tetra chloropalladate (II) (MTCP) [5], morpholinium oxalate (MO) [6], 4-Methylmorpholine (4 MM) [9], Morpholin-4-ium hydrogen tartrate (MHT)[10], 4-Morpholinium bis(hydrogen squarate) (4MBHS) [11] and Morpholinium 2-chloro-4-nitrobenzoate (M2C4N) [12] utilizing experimental spectroscopic methods, DFT simulations, and NLO effects. The structural geometry and vibrational spectra of a compound were analyzed and reported in both theoretical and experimental techniques. The natural bond orbital (NBO) analysis was used to investigate interactions between molecules, including intermolecular charge transfer and hydrogen bonding interaction. The global reactivity parameters have been calculated by Frontier molecular orbital (FMO) analysis. A molecular electrostatic potential (MEP) map was used to assess the chemical reactivity of the molecule. UV-visible spectral analysis has been carried out to identify the various possible electronic transitions. Utilizing the Electron Localization Function (ELF), Localized Orbital Locator (LOL), and Reduced Density Gradient Analysis (RDG), which provides details on both inter and intra non-covalent interactions, the chemical significance of the molecule was described. Density Overlap Region Indicator Analysis (DORI) and Hirshfeld analysis were used to study the charge transfer interaction. The dipole moment (μ), linear polarizability (α) first and second order hyperpolarizability (β) values have been computed.

2. Experimental details

Single crystals of MP were grown by the slow evaporation solution growth technique. Morpholine with Perchloric acid was taken in the stoichiometric ratio of 1:1 by dissolving in a mixture of ethanol and deionized water which is stirred well to make a homogeneous solution after two hours the white precipitate was obtained. The precipitate is allowed to dry and used for the further growth of MP. The synthesized material was purified by the repeated recrystallization process, the single crystals of MP were harvested from mother solution after a growth period of 45days [8]. FT-IR spectrum be recorded using a SHIMAZDU infrared spectrometer employing KBr pellet technique in the frequency region 4000 to 400 cm^{-1}. The electronic absorption spectrum was measured using Perkin-Elmer Lambda 35 spectrometer in the range of 200–1100 nm. Detailed experimental studies were reported in the previous work [8]. FT-Raman spectrum in the wavenumber range 3500–50 cm^{-1} was recorded by the BRUKER RFS 27: FT-Raman spectrophotometer using Nd: YAG laser at 1064 nm as the excitation source with resolution of 2 cm^{-1}.

3. Computational details

The quantum chemical computations of MP have been accomplished using a level of theory augmented with the standard B3PW91/6–31 G (d, p) [13] basis set, using the Gaussian'09 software package [14]. Natural bonding orbital (NBO) analysis has been performed using NBO 3.1 program [15] at the same level to interpret the electronic structure and the formation of intramolecular and intermolecular hydrogen bonds. Normal coordinate analysis (NCA) has been performed and the assignment of the vibrational modes has been carried out on the basics of Potential Energy Distribution (PED) using the MOLVIB7.0 program as described by Sundius [16,17]. Hirshfeld surfaces were examined using the Crystal Explorer program [18]. All density overlap regions indicator analysis and density of states analysis were performed using Multiwfn, which is a multifunctional wave function analysis program [19], and all isosurface maps were rendered by the Visual Molecular Dynamics (VMD) program [20]. Calculations for hyperpolarizability utilized the same basis set.

4. Results and discussion

4.1. Molecular optimization

To get essential structural characteristics, MP has been optimized using B3PW91/6–31 G (d,p) level theory. The experimental data for MP is correlated with XRD data (CCDC No: 910,879) [8] and also compared with the experimental value of morpholinium tetra chloropalladate (II) (MTCP) [5] and morpholinium oxalate (MO) [6]. Table S1shows the bond lengths of MP, MO and MTCP, while Table S2 provides information on the bond angle and dihedral angle of MP.The optimized structure in Fig. 1 uses the MP atomic numbering system and is held together by doubly hydrogen-bonded interactions that were calculated using DFT.

Bond length of N2-H3 (0.9 Å) and N2-H4 (0.9 Å) in MP is deviates from the standard value 1.08 Å [21] and also the effect of ionic interactions from the NH_2^+cation to the ClO_4^-anion as evidenced from Table S1. The internal angles of the morpholinium ring in MP the calculated values of C8-O1-C14 (110.14°), C5-N2-C11 (110.30°), N2-C5-C14(108.37°), O1-C8-C11(110.02°), N2-C11-C8 (108.37°) and O1-C14-C5 (110.51°) significantly deviated from the expected trigonal angle (120°) because of the effect of hyperconjugative interactions the C—H bond length of methylene groups. The N2…O18 distance indicates strong N—H…O hydrogen bonding, and this length is shorter than the van der Waals separation between the O atom and the H atom [22]. The calculated bond length of Cl17-O18 (1.524 Å) and Cl17-O20 (1.506 Å) is greater than the experimental bond length of 1.373 Å and 1.438 Å due to the intermolecular hydrogen bonding interaction. The charge on the morpholinium cation gets balanced by the perchlorate anion outside the coordination sphere. The perchlorate anion is highly distorted from its tetrahedral arrangement as evidenced by its bond angles of O18-Cl17-O21 (109.516°), O19-Cl17-O20 (109.05°), O19-Cl17-O21 (112.61°) and O20-Cl17-O21 (110.68°) respectively. The geometry of the N—H…O hydrogen bond in MP may be characterized by the torsion angles H4-N2-H3-O20, H3-N2-C11-C8 and C5-N2-H3-O20,which are equal to 15.078°, 133.69° and −98.418° respectively. Most of them are in agreement with the experimental values, but the bond length C11-N2 in MP (1.465 Å) is less than that of MO (1.489 Å) and MTCP (1.488 Å) due to the typical double bond character [23]. Bond length of N2-H3 (0.900 Å) and N2-H4 (0.900 Å) in MP is marginally improved from MO (0.8900 Å) and MTCP (0.8200 Å) is due intermolecular hydrogen bonding interactions. C—C bond lengths in MP (1.496 Å and 1.522 Å), MO (1.5069 Å and 1.5091 Å), and in MTCP (1.492 Å and 1.497 Å) are shortened from the normal bond length 1.57 Å owing to the steric effect of the lone-pair electron predicted by valence-shell electron-pair repulsion theory (VSEPR) [24].

4.2. Natural bond orbital analysis

An NBO analysis of MP has been done to understand the charge-transfer interactions. Table 1 shows the stabilization energies (donor-acceptor interactions) of the MP using second order perturbation of the Fock matrix method. When stabilization energy E(2) is high, the donor and acceptor interactions will be very intense.

The magnitudes of charge transferred from lone pairs of the hydrogen bonded oxygen atoms into the σ*(N—H) being the H-donors, these lone pair electrons which are transferred from $n_1O_{18}\rightarrow \sigma^*(N_2—H_4)$ and $n_1O_{20}\rightarrow \sigma^*(N_2—H_3)$ respectively, are evident for the non-covalent hydrogen bonding ($N_2—H_4…O_{18}$ and $N_2—H_3…O_{20}$) which is significant in the improvement of the optical activity of this compound. The stabilization energy E(2) is associated with hyperconjugative interactions $n_1O_{18} \rightarrow \sigma^*(N_2—H_4)$, $n_1O_{18} \rightarrow \sigma^*(N_2—H_4)$, $n_1O_{20} \rightarrow \sigma^*(N_2—H_3)$, $n_1O_{20} \rightarrow \sigma^*(N_2—H_3)$ and $n_1O_{18}\rightarrow \sigma^*(C_{11}—H_{12})$ are obtained as 9.82, 32.66,4.84, 11.01 and 0.28 kcal/mol respectively which quantify the extend of non-

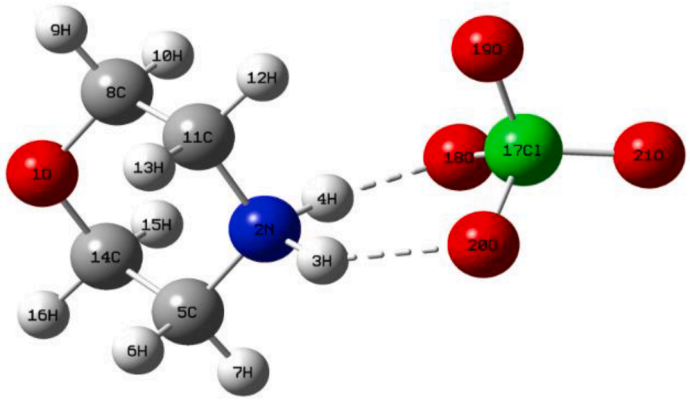

Fig. 1. Optimized structure of MP.

Table 1
Second order perturbation theory analysis of Fock matrix in NBO basis.

Donor(i)	Occupancy ED	Acceptor(j)	Occupancy ED	E(2)[a] Kcal/mol	E(j)-E(i)[b] (a.u)	F(i,j)[c] (a.u)
$\sigma(N_2—H_4)$	1.98070	$\sigma^*(Cl_{17}—O_{18})$	0.28998	0.20	0.80	0.012
$\sigma(N_2—H_4)$	1.98070	$\sigma^*(Cl_{17}—O_{21})$	0.22454	0.08	0.87	0.008
$\sigma(Cl_{17}—O_{18})$	1.97988	$\sigma^*(N_2—H_4)$	0.09809	0.26	1.26	0.016
$\sigma(Cl_{17}—O_{20})$	1.98048	$\sigma^*(N_2—H_4)$	0.09809	0.15	1.29	0.012
$\sigma(Cl_{17}—O_{21})$	1.98242	$\sigma^*(N_2—H_4)$	0.09809	0.08	1.34	0.010
$\sigma(C_5—H_7)$	1.97974	$\sigma^*(O_1—C_{14})$	0.01793	3.86	0.84	0.051
$\sigma(C_5—H_7)$	1.97974	$\sigma^*(N_2—C_{11})$	0.02461	3.53	0.81	0.048
$\sigma(C_{14}—H_{16})$	1.97882	$\sigma^*(N_2—C_5)$	0.02631	4.23	0.80	0.052
$\sigma(O_1—C_8)$	1.98985	$\sigma^*(C_{14}—H_{16})$	0.01286	1.53	1.28	0.039
$\sigma(N_2—H_3)$	1.98332	$\sigma^*(C_8—C_{11})$	0.02568	2.16	1.03	0.042
n_1O_{18}	1.96859	$\sigma^*(N_2—H_4)$	0.09809	9.82	1.15	0.097
n_1O_{20}	1.97664	$\sigma^*(N_2—H_3)$	0.04903	4.84	1.22	0.069
n_2O_1	1.91755	$\sigma^*(C_5—C_{14})$	0.02709	6.97	0.65	0.061
n_2O_1	1.91755	$\sigma^*(C_{14}—H_{15})$	0.02839	5.81	0.73	0.059
n_3O_{18}	1.81817	$\sigma^*(N_2—H_4)$	0.09809	32.66	0.68	0.135
n_3O_{20}	1.83303	$\sigma^*(N_2—H_3)$	0.04903	11.01	0.68	0.080
n_1O_{19}	1.98471	$\sigma^*(C_{11}—H_{12})$	0.01422	0.28	1.29	0.017
n_1O_1	1.96635	$\sigma^*(C_5—C_{14})$	0.02709	1.23	0.93	0.030
n_1O_1	1.96635	$\sigma^*(C_8—C_{11})$	0.02568	1.16	0.94	0.030

[a] E(2) means energy of hyper conjugative interactions.
[b] E(j)-E(i) Energy difference between donor and acceptor i and j NBO orbitals.
[c] F(i,j) is the Fock matrix element between i and j NBO orbitals.

covalent hydrogen bonding. The differences in E(2) energies are probably due to the fact that the accumulation of electron density in the N—H bond is not only drawn from the n(O) of the hydrogen acceptor but also from the entire molecule. The covalent molecular charge transfer from the CH_2 group, NH_2 group to the morpholinium ring is revealed by the interaction of the methyl orbitals $\sigma(C_5—H_7)\rightarrow\sigma^*(O_1—C_{14})$, $\sigma(C_{14}—H_{16})\rightarrow\sigma^*(N_2—C_5)$, $\sigma(N_2—H_3)\rightarrow\sigma^*(C_8—C_{11})$ with the stabilization energy 3.86,4.23 and 2.16 kcal/mol respectively.

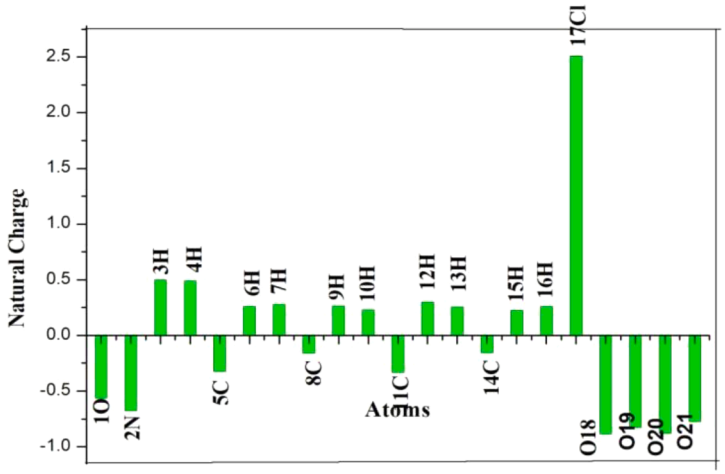

Fig. 2. Natural population analysis of MP.

4.3. Natural population analysis

The plot of the natural charges of the MP molecule is presented in Fig. 2 and the natural charges are listed in Table S3. The hydrogen atoms of the amino group are found to have a high positive charge (H3: 0.49875e and H4: 0.48917e) when compared with other hydrogen atoms. This is due to a cooperative effect between the donor and acceptor associated with a conspicuous contraction in H…O that provides stability to the system. A nitrogen atom N2 becomes negative charge because of the interaction of N—H…O and carbon atoms, an oxygen atom of morpholinium ring has a negative charge.

The tetrahedral ClO_4 bonds such that the chlorine atom Cl17 has a high positive charge (2.5098e) due to that more protons are occupied the perchlorate anion moiety [25]. Hence, theoxygen atoms O18, O19, O20, and O21 bonded with chlorine becomes more electronegative.

4.4. Vibrational analysis

FT-IR and FT-Raman spectral wavenumbers have been assigned based on the normal coordinate analysis following the scaled quantum mechanical force field methodology. The title molecule consists of 21 atoms, which gives rise to 57 normal modes of vibrations. The observed IR band with its relative intensities and calculated scaled wavenumbers and assignments are given in Table S4 and the FT-IR and FT-Raman spectrum of MP is shown in Figs. 3 and 4.

4.4.1. NH_2 vibrations

The hetero aromatics holding a NH_2 group stretching vibrations in the region 3500–3220 cm^{-1} and the position of absorption in this general region are connected with hydrogen bonding [26,27]. In MP, the symmetric stretching vibration of NH_2 cation is observed as medium and weak band in FT-IR and in Raman at 3415 cm^{-1} with the scaled value at 3417 cm^{-1} whereas the asymmetric stretching vibrations of NH_2 cation appears as a very strong band in FT-IR at 3059 cm^{-1} and FT-Raman at 3057 cm^{-1} with the scaled value at 3061 cm^{-1}. This band show the level of intermolecular hydrogen bonding N—H…O with the formation of NH_2 cation by accepting an oxygen atom from the perchlorate moiety. In FT-Raman spectra, NH_2 in-plane bending vibrations are seen as a weak band at 1655 cm^{-1}, and out-of-plane bending vibrations are seen as a medium band at 1453 cm^{-1}. Scaled frequencies for the in-plane and the out-of-plane bending vibrations occur at 1662 and 1474 cm^{-1} respectively and are related to the experimental values.

4.4.2. CH_2 vibrations

The CH_2 asymmetric and symmetric stretching vibrations come around in the range of 3100 and 3000 cm^{-1} [26,27]. In MP, asymmetric CH_2 stretching vibrations are observed as a medium band at 3282 cm^{-1}

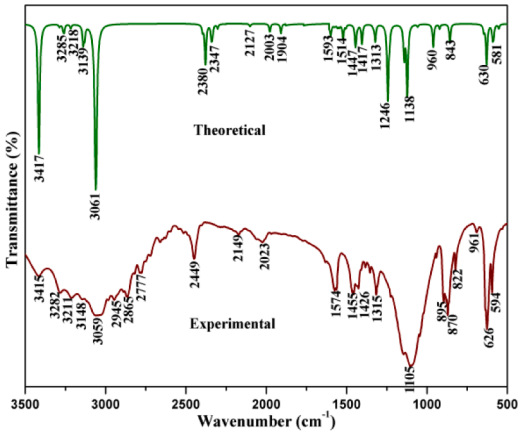

Fig. 3. Experimental and Simulated FT-IR spectra.

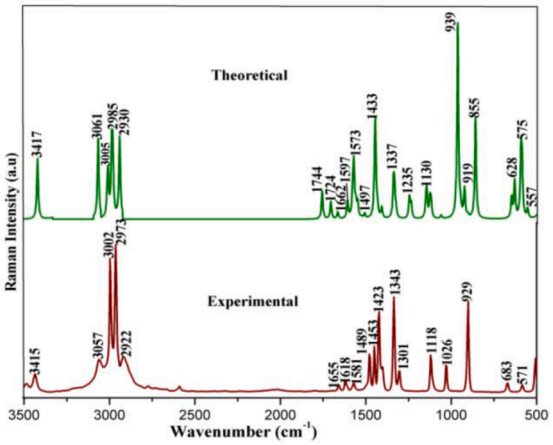

Fig. 4. Experimental and Simulated FT-Raman spectra.

in FT-IR and weak band at 3095 cm^{-1} in FT-Raman which concurs with the scaled value. This increase of frequency is because of the CH_2 located on the morpholinium ring this makes the oxygen atom in ether functional group has lone pair of electrons and the substituent nitrogen atom in NH_2 group in shifting the CH_2 bands [28]. These shift also due to the weak van der Waals interaction which enables the C—H bond to retrench, as evidenced by DORI analysis. In MP, symmetric CH_2 stretching vibrations are observed as a very strong band at 3002 cm^{-1} in FT-Raman and weak band at 3211 cm^{-1} and 3148 cm^{-1} in FT-IR which concurs with the scaled value. In MTCP, the asymmetric stretching vibration is observed as a weak band at 2961 cm^{-1} and this less intense is due to the presence of hydrogen bonding [5]. Normal value of CH_2 in-plane bending vibration of morpholinium ring 1482–1446 cm^{-1} [29] which is observed in FT-Raman at 1423 cm^{-1}. In the title compound, CH_2 rocking and CH_2 twisting vibrationsare observed in FT-Raman at 1332 cm^{-1} and IR at 1143 cm^{-1} which are compared with 4 MM [9] molecule are 1329 cm^{-1} in FT-Raman and 1154 cm^{-1} in IR respectively which infers that the band has affected by the methyl group attached to the morpholinium ring in 4 MM.

4.4.3. C-C, C-N and C-O vibration

Morpholinium ring has two C—C, C—N and C—O stretching vibrations which are more substituent dependant. C—C stretching vibration in MP as very strong band at 907 cm^{-1} in FT-IR relates to the scaled at 919 cm^{-1} and C—O stretching vibrations are observed as 1455 and 1105 cm^{-1} in FT-IR and 1082 cm^{-1} in FT-Raman agrees with the scaled at 1413 and 1092 cm^{-1} which is down shifted depending on neighbouring group, conjugation effects, H-bonding and molecular tautomerism [30]. C—C stretching modes in MO [6] at 1394 cm^{-1} in FT-Raman and C—O stretching vibrations observed at 1100 cm^{-1} in FT-IR and 1110 cm^{-1} FT-Raman. The morpholinium ring C—N stretch is usually coupled with the C—C and C—O stretch. In MP, the C—N stretching observed at 1315 cm^{-1} in FT-IR and 1119 and 1082 cm^{-1} in FT-Raman which is agree well with the scaled values at 1318 cm^{-1}, 1130 cm^{-1} and 1092 cm^{-1} this indicates strong N—H…O hydrogen bonding. The C—N stretching vibrations in MO [6] at 1041 cm^{-1} in FT-IR and 1015 cm^{-1} in FT-Raman it evidenced the morpholinium ring is attached to the oxalate anion moiety in MO. The C—N stretching vibrations in 4 MM [9] at 1257 cm^{-1} in FT-Raman and 1141 cm^{-1} in FT-IR it implies that the methyl group connected to the morpholinium ring in 4 MM. The hyperconjugative covalent molecular charge transfer from the amino group, NH_2 group to the morpholinium ring $\sigma^*(O_1—C_{14})$, $\sigma^*(N_2—C_5)$ and $\sigma^*(C_8—C_{11})$ which isrevealed by NBO analysis is clearly reflected in FT-IR and FT-Raman spectra showing a downshift of C—C, C—N, C—O stretching mode.

4.4.4. ClO_4^- vibrations

The asymmetric and symmetric stretching vibrations for the ClO_4^- ion

normally observed at the range 1100 cm^{-1} and 936 cm^{-1} respectively [31]. For MP, symmetric stretching vibrations for the ClO_4^- ion observed as medium to very strong peak in FT-Raman at 1119 cm^{-1} and 919 cm^{-1} which is well correlated with scaled wavenumbers at 1138 cm^{-1}, 1130 cm^{-1} and 939 cm^{-1} whereas weak asymmetric stretching vibration observed at 1247 cm^{-1} in FT-Raman related with scaled value 1235 cm^{-1}. Variations in ClO_4^- stretching frequencies are attributed to the position of perchlorate bands strongly supports the coordination of azomethine -C=NH_2 nitrogen to the morpholinium ring that exhibits broad spectrum optical activities [32]. Also, the shift has been validated by the second order perturbation energy that takes place between $LP_1O_{18}\rightarrow \sigma^*(N_2—H_4)$ and $LP_1O_{20}\rightarrow\sigma^*(N_2—H_3)$ with the stabilization energy of 9.82 and 4.84 kcal/mol and the occupancy of the interacting NBOs. Presumably, the symmetry change from ClO_4 to ClO_3 allows the symmetric bending vibration to become FT-IR active. The symmetric deformation mode of coordinate ClO_3 group is observed as medium band at 551 cm^{-1} and 533 cm^{-1} in FT-IR and very weak band at 550 cm^{-1} and 533 cm^{-1} in FT-Raman [31]. In MP, the symmetric bending mode of coordinate group ClO_3^- is observed as very strong band at 626 cm^{-1} in FT-IR and weak to medium band at 672 cm^{-1} and 478 cm^{-1} in FT-Raman. The scaled wavenumber assigned at 701 cm^{-1}, 628 cm^{-1} and 478 cm^{-1} which is corresponds to umbrella and scissoring mode respectively.

4.5. Frontier molecular orbital analysis

Frontier molecular orbital analysis is used to investigate the inter and intra-molecular charge transfer between electron donor and electron acceptor groups through a conjugated route [32]. Fig. 5 shows the HOMO-LUMO plot of MP computed at different levels of theory, where the positive phase is exhibited in red and negative phase is depicted in green. The frontier molecular orbital gap exposes information about the molecule's chemical reactivity and kinetic stability [33].

The HOMO-LUMO plot shows that the HOMO is localized only on the electron withdrawing ClO_4^-anion while the LUMO is localized on the electron accepting NH_2, C—C, C—N and C—O bonds in the morpholinium ring. The HOMO and LUMO energy gap found to be 6.38 eV which is correlated the experimental energy gap found to be 6.2 eV indicates high kinetic stability and low chemical reactivity. It explains the ultimate ionic charge transfer interaction taking place from ClO_4 anion to the morpholine cation to form morpholinium perchlorate required for optical activity [34]. To evaluate the energy gaps that the range separated and global hybrid MP functions predicted. The energy gap can be roughly calculated using the difference between the lowest unoccupied and highest occupied molecular orbital energies based on the Kohn-Sham theory [35]. E_{LUMO}, E_{HOMO}, and the ionization energies (IE) for the MP estimated at the B3PW91/6–31 g(d,p), B3LYP/6–31 g(d,p), CAM-B3LYP/6–31 g(d,p), and B3LYP/CC-PVDZ levels of theory are compared in Table 2. It is well known from Kohn-Sham theory that a "perfect functional" (assuming one had access to one) would produce an ionization energy precisely equal to E_{HOMO}. These results show that a full 100% asymptotic contribution of HF exchange is required to provide a consistent explanation of the electrical characteristics in these systems, complementing excitation energies. Additionally, these results show that the range-separated formalism with full asymptotic HF exchange is remarkably self-consistent because it accurately predicts both of the excitation energies in these systems while also satisfying the necessary energy restrictions [36,37].

Table 2 depicts the information about global reactivity of MP such as chemical hardness, softness, electronegativity, chemical potential, and electrophilicity index calculated by HOMO-LUMO energies. Chemical hardness calculated to be 4.139 eV upholds the stability of compound whereas electronegativity describes the ability to induce the shared electrons, is found to be 3.193 eV. Electrophilicity index calculated to be

Table 2
Calculated energy values of MP for different basis sets.

Parameters	B3PW91/ 6–31 G (d,p)	B3LYP/ 6–31 g(d, p)	CAM-B3LYP/6–31 g(d,p)	B3LYP/ CC-PVDZ
E_{HOMO}(eV)	−5.385	8.112	6.502	7.151
E_{LUMO} (eV)	0.946	0.848	1.207	0.370
Energy gap (eV)	6.387	7.269	5.294	6.78
Ionization Energy I (eV)	5.385	−8.112	−6.502	−7.151
Electron Affinity A (eV)	−0.946	−0.848	−1.207	−0.370
Electronegativity(χ) (eV)	3.193	−4.48	−3.854	−3.760
Chemical potential (μ) (eV)	−4.139	−3.634	−2.647	−3.39
Chemical hardness (η) (eV)	4.139	3.634	2.647	3.39
Chemical softness (S) $(eV)^{-1}$	0.120	0.137	0188	0.147
Electrophilicity index (ω) (eV)	2.069	1.816	1.323	1.694

Table 3
HOMO-LUMO energy gap values of Morpholinium derivatives.

Compounds	Energy gap (eV) Theoretical
MP	6.38
MO [6]	5.15
4 MM [9]	5.93
MHT [10]	5.64
4MBHS [11]	4.41
M2C4N [12]	9.38

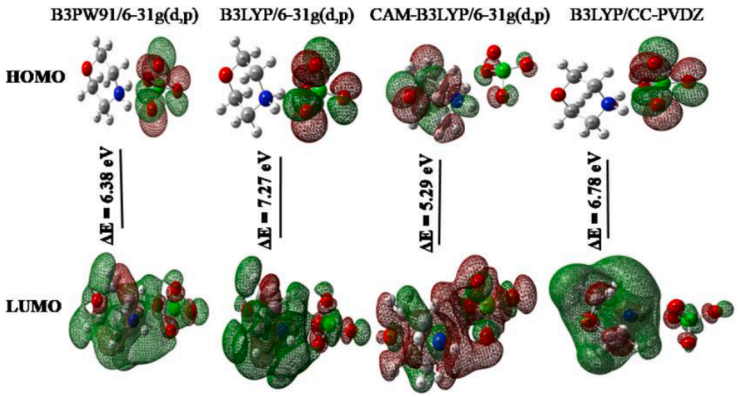

Fig. 5. Frontier Molecular Orbitals of MP.

2.069 eV emphasizes optical activity [38,39]. The energy gap values of MP in comparison with morpholinium derivatives are tabulated in Table 3. The theoretical energy gap values are in the order M2C4N > MP > 4 MM > MHT > MO > 4MBHS.

4.6. UV–vis analysis

The propensity of compounds to absorb UV and visible light radiation is investigated employing UV-visible analysis. UV-visible spectrum investigation has been performed experimentally with DMSO as a solvent is provided in Fig. 6a.

UV–vis excitation energy and oscillator strength for MP portrayed in Table 4. The absorbance of light in the UV region contains the movement of electrons from the ground to higher states in σ and π orbitals. The experimental spectrum reveals two absorbance bands around 200 nm and 332 nm were attributed to π→π* and n→π* transitions. But the theoretical band at 156 nm (with oscillator strength $f = 0.0297$) with major contributions from H-2→LUMO (68%), H-2→$L + 1$ (20%). The shift between calculated and experimental energies ismainly attributed to the hydrogen bonding interactions between MP and solvent molecules including explicit and implicit solvent model [40]. Tauc's plot is the traditional method E_g for estimation from UV–vis data [41]. The direct and indirect band gap of the MP was analysed by plotting as shown in Fig. 6b and 6c and it was found to be 3.5 eV and 3.8 eV. The Tauc's plot is unarguably appropriate and yields reasonable values of E_g when correctly applied. The direct and indirect optical band gap of MP is traditionally measured by extrapolating the linear region, developed by Tauc, has also been widely used [42].

4.7. Molecular electrostatic potential (MEP) analysis

MEP is a very significant characteristic because it offers a depth of knowledge regarding the chemical reactivity of the investigated substance, particularly when describing intermolecular interactions. To evaluate the reactive areas for electrophilic and nucleophilic assaults, MEP investigations were conducted. Fig. 7 shows that the negative (red and yellow) and positive (blue) sections of the MEP are related to electrophilic and nucleophilic reactivity, respectively.

Negative electrostatic potential is localized over oxygen atoms in ClO_4^- group perchlorate anion is most reactive site for electrophilic attack whereas positive electrostatic potential is localized over electropositive hydrogen atoms of morpholinium ring making them reactive sites for nucleophilic attack. The site around these shows the formation of inter-molecular interactions as evinced by optimized and NBO analysis. Natural population analysis also validates that oxygen atoms have high negative charge favourable for electrophilic attack and that the high positive charge of hydrogen atoms makes them favourable for nucleophilic attack. Electron rich morpholinium ring cation makes it as a hydrogen bond donor and perchlorate anion acts as a hydrogen bond acceptor.

4.8. Hirshfeld analysis

Hirshfeld surface analysis describes the hydrogen bonding existence and closer contacts in the solid state structure of the molecules and intermolecular interactions based on the value of d_{norm} (normalized contact distance) and corresponding finger print plots, which are recent

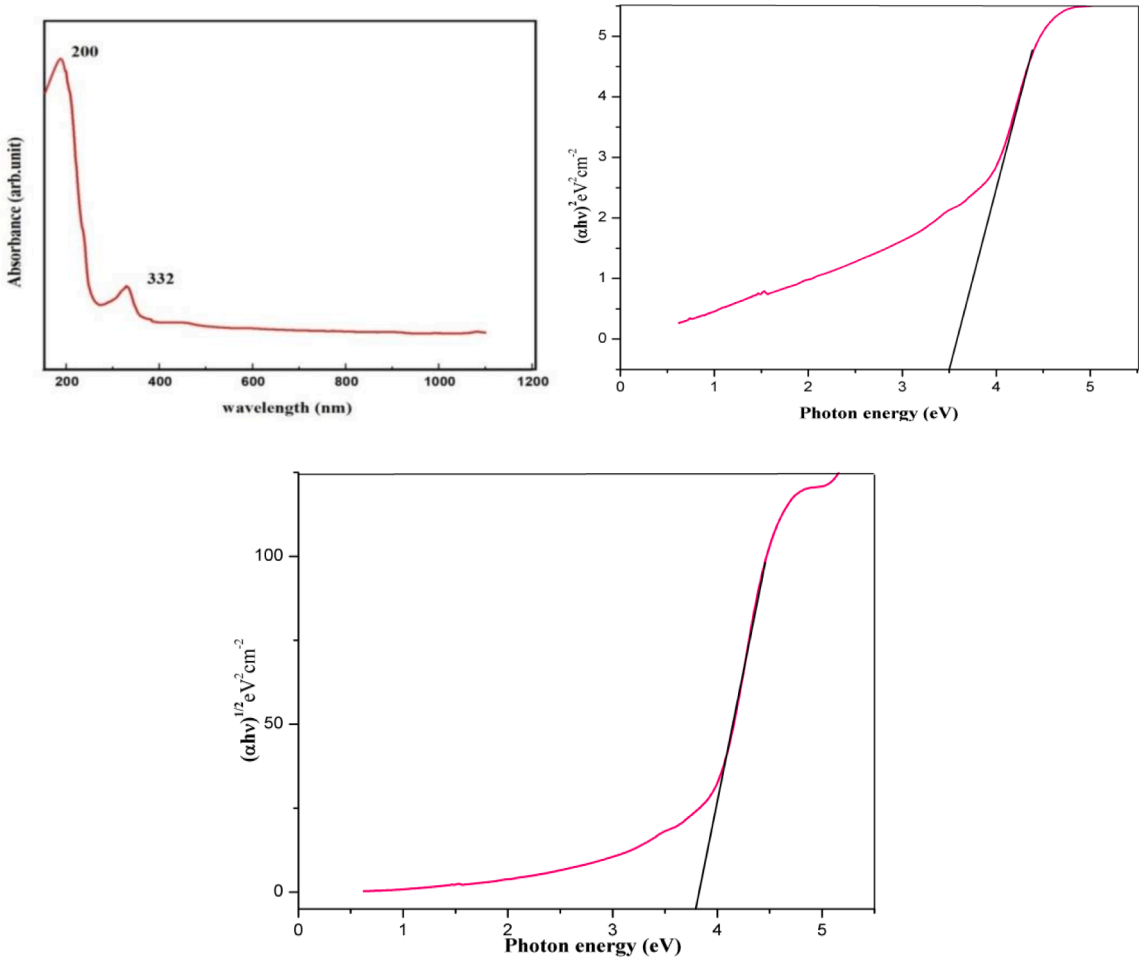

Fig. 6. (a) Experimental UV absorbance spectra of MP. (b) Direct Tauc plot of MP (c) Indirect Tauc plot of MP.

Table 4
UV–vis excitation energy and oscillator strength for MP.

States	Experimental		TD-DFT/ B3PW91/6–31G(d,p)				Major contributions
	λ_{max} (nm)	Band gap (eV)	λ_{max} (nm)	Band gap (eV)	Energy (cm^{-1})	f (O.S)	
S1			174	7.12	62,117	0.0007	HOMO→LUMO(66%), HOMO→$L+1$ (17%)
S2			173	7.16	62,252	0.0019	H-1→LUMO(62%), H-1→$L+1$ (24%)
S3	200	6.2	156	7.94	63,917	0.0297	H-2→LUMO(68%), H-2→$L+1$ (20%)

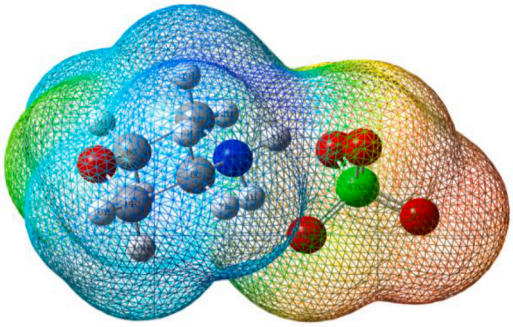

Fig. 7. Molecular electrostatic potential map of MP.

approaches in molecular crystals. The d_{norm} is found by seeing the global relation among the distances of some surface points to the nearest interior (d_i) and exterior (d_e) atoms and the van der Waals radii of the atoms [43]. The Hirshfeld surface of the molecule mapped over d_{norm} is shown in Fig. 8. The closer contacts with longer and shorter distances of van der Waals radii are represented in blue and red respectively. The bright red region on the Hirshfeld surface is due to N—H…O non-covalent interaction and pale red region is owing to the presence of weak C—H…O non-covalent interaction.

The 2D fingerprint plots are used to understand the atom pair intermolecular interactions in a crystal structure [44]. The relative contributions of different individual contacts to the overall Hirshfeld surface are given in Fig. 9. The color of each point: blue, green, and red correspond to small, moderate, and high contributions whereas an uncolored region indicates no contributions to the Hirshfeld surface. The O…H contacts with a contribution of (74.2%) appear as two sharp spikes on the fingerprint plots, which is indicative of strong hydrogen bond interactions. The H…H contacts contribute (20.2%) to the total Hirshfeld surface area in the middle region. The obtained plots are used to describe various interactions, including O—O (5.5%) and other contacts present in the crystal structure.

4.9. ELF and LOL analysis

Electron localization function (ELF) and localized orbital locator (LOL) are the useful tools which help to identify the regions of lone pairs, bond pairs and size of the bonding the title molecule [45]. Color map of

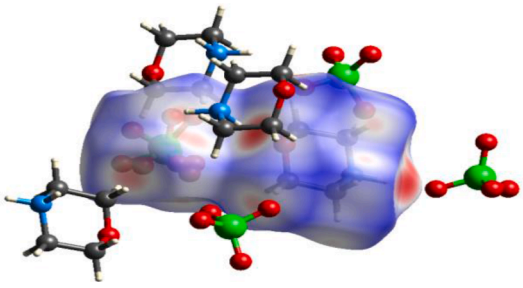

Fig. 8. d_{norm} mapped on Hirshfeld surfaces for visualizing the intermolecular interactions.

ELF and LOL gives information about electron density charge distribution whereas the two dimensional color shade maps are given in Fig. 10.

In Fig. 10a, the high ELF regions were seen around the hydrogen atom indicated the high localization of boding and non-bonding electrons. The blue region was present around carbon and oxygen atom which show the presence of delocalized electrons cloud. From the Fig. 10b, covalent regions were seen between carbon and carbon atoms of the morpholine ring which were indicated by red color with high LOL value.

4.10. Reduced Density Gradient (RDG) analysis

The molecular stability was ensured by non-covalent interactions with inter and intramolecular interactions were predicted using the RDG analysis based on the non covalent interaction (NCI) method [46]. The λ_2 sign was exploited to differentiate between the bonded ($\lambda_2<0$) and non−bonded ($\lambda_2>0$) interactions. In MP molecule, the λ_2 sign ρ function ranges from −0.05 to 0.05 a.u. in the RDG scatter graph depicted in Fig. 11.

The function of λ_2 (r) chooses between −0.035 and 0.020 a.u in the RDG scatter plot, which are allocated to red, green and blue. In the RDG isosurfaces, the red spike shows the steric repulsion perceived in the centres of the morpholinium ring. The RDG scatter graph manifests the red contour between 0.02 a.u and 0.015 a.u, indicating the higher repulsive exchange contribution. This plot illustrates the steric repulsive force between the ionic chlorine and nitrogen. Hydrogen bonding interaction N—H…O illustrates the attractive force between and is exposed by the bluish spikes. The presence of strong hydrogen bonding interaction is established in the scatter graph for NCI between −0.025 a.u and −0.035 a.u in the bluish domain. C—H…O hydrogen bonding formation due to the interaction between oxygen atoms and the anionic perchlorate group is deep-rooted between 0 a.u and 0.010 a.u domains. Interacting regions in the MP molecule make the isosurface plot clearer through the NCI scatter plot. RDG analysis does not show the RDG domains between the covalently bonded atoms in the molecule.

4.11. Density Overlap Regions Indicator (DORI) analysis

DORI analysis offers difference between covalent and non-covalent contacts in molecular structure. DORI scheme the colourful spheres visualize the areas of a different types of interactions dependent on their strength. Various molecular phenomena concerning visualization of covalent bonding patterns, steric clashes as well as of typical non-covalent interactions occurring between and within molecules characterizethe utility of DORI analysis [47]. The isosurface density plot of DORI analysis is as shown in Fig. 12.

The interacting sites may be identified using a DORI enclosing their real space, with blue, green, and red areas representing the H-bond interactions, van der Waals interactions, and steric impact, respectively. Red color indicates the steric effect is localized in center of morpholinium ring whereas green color indicates the presence of weak non-covalent C—H…O interaction. Blue color indicates stronger attractive interaction corresponding to strong non-covalent hydrogen bonds (N—H…O). The covalent bond regions are revealed by blue surfaces, which validate the vast electron density and the strong bonding effect in these regions. The carbon-carbon, carbon-nitrogen, carbon-oxygen and

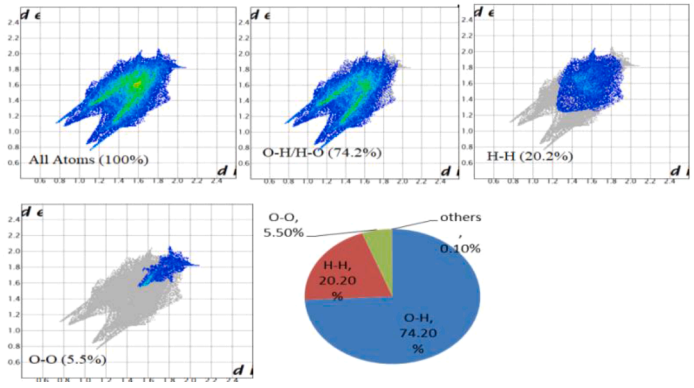

Fig. 9. 2D fingerprint plots of different atom…atom contacts and their relative contributions.

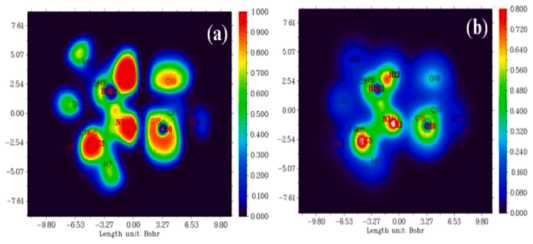

Fig. 10. (a) ELF and (b) LOL color filled map for LF.

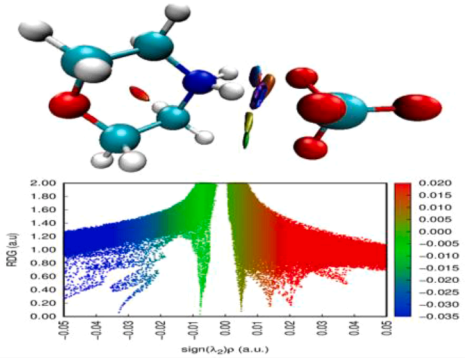

Fig. 11. 2D scatter plot and 3D RDG isosurface densities of MP.

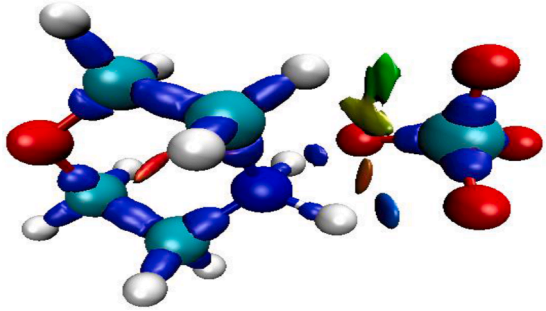

Fig. 12. Isosurface plot of DORI analysis.

chlorine-oxygen covalent contacts in morpholinium perchlorate molecule are established.

4.12. NLO effects

Researchers have been interested in the photophysical characteristics, NLO characteristics, and dyeing applications of various dyes [48]. The NLO parameters are represented in Table 5 and include the total dipole moment, dynamic average linear polarizability, average first and second order hyperpolarizability.

The calculated total dipole moment value of MP was 3.701 Debye and a dynamic average linearpolarizability value was 11.8192×10^{-24} e.s.u. The calculated average linear polarizability value is 1.62 times larger than the NLO reference material KDP (7.28×10^{-24} e.s.u), due to the strong donor and acceptor of MP molecule which increases their linear polarizability and contingent that strong charge transfer within the molecule. These charge transfer induced the high nonlinearproperty of the title molecule. The first order hyperpolarizability measures the NLO activity of MP. The first and second order hyperpolarizability of MP is 2.6061×10^{-30} e.s.u., 1.16675×10^{-39} e.s.urespectively. The calculated value of polarizability shows more NLO active nature of MP while comparing with other related compounds. Table 6 contains the MP and its associated compound's computed first and second order hyperpolarizability. The increase of first order hyperpolarizability value with increase in substitution in the order MP > MHT > M2C4N > 4MBHS > MO > 4 MM may lead to a better polarity with a high energy gap. The increase in dipole moment, linear polarizability, first and second order polarizability provides better polarity in the MP molecule due to its donor group and intermolecular interactions.

5. Conclusion

The compound MP has been characterized by FT-IR and FT-Raman spectroscopic techniques using DFT calculations and the complete vibrational analysis has been carried out. Optimized geometry and NBO analysis confirm the formation of two inter-molecular interactions which is important for the optical activity is evidenced from the transfer of electrons from the lone pair oxygen in ClO_4^-anion group to the antibonding orbital of NH_2^+cation group in morpholinium ring. The occurrence of N—H…O intermolecular interactions and the conspicuous red shifting in the wavenumber have been authenticated by the increase in N—H bond length and an increase in the electron density in the antibonding orbitals. The morpholinium ring stretching modes downshifted because of the hyperconjugative intra-molecular interaction. The value of the HOMO-LUMO energy gap enhances the intermolecular charge transfer interaction within the molecule, leading to a better nonlinear optical response similar to other morpholinum derivatives. MEP plot and natural population analysis confirms that ClO_4 groups are site for electrophilic attack and hydrogen atoms in morpholinium ring is most

Table 5
Dipole moment, Polarizability, First and Second Polarizabilities of MP.

Dipole moment μ (Debye)	Polarizability (α(-ω;ω))(x10^{-24}e.s.u)		First Polarizability (β(-ω;ω,0)) (x10^{-30}e.s.u)		Second Polarizability (γ(-ω;ω,0,0)) (x10^{-40}e.s.u)		
μ_x	−3.628963	α_{xx}	93.5796563	β_{xxx}	−264.2245	γ_{xxxx}	−8.58226
μ_y	−0.451127	α_{xy}	1.7471964	β_{xxy}	−9.251052	γ_{xxyy}	6.0674751
μ_z	0.571081	α_{yy}	77.4190649	β_{xyy}	−17.09366	γ_{yyyy}	2.5147849
		α_{xz}	−2.1667673	β_{yyy}	−23.50198	γ_{yyzz}	2.7851817
		α_{yz}	0.8693381	β_{xxz}	59.206013	γ_{zzzz}	−0.233243
		α_{zz}	68.2580107	β_{xyz}	−4.400596	γ_{zzxx}	0.0889958
				β_{yyz}	−1.944985		
				β_{xzz}	−9.743335		
				β_{yzz}	−4.475902		
				β_{zzz}	12.783611		
(μ)	3.701	(α(ω;ω))	11.8192	(β(-ω;ω,0))	2.6061	(γ(-ω;ω,0,0))	11.6675

Table 6
Calculated value of polarizabilities, first and second order hyperpolarizability moment in MP and its related compounds, urea, KDP at DFT level.

Compounds	μ (Debye)	$\Delta\alpha \times 10^{-24}$ (esu)	$\beta \times 10^{-30}$ (esu)	$\gamma \times 10^{-39}$(esu)
MP	3.7012	11.8192	2.6061	1.16675
MO[6]	9.25	−7.427	0.817	–
4 MM [9]	1.44	0.795	0.496	–
MHT[10]	5.44	5.86	2.46	0.02194
4MBHS[11]	10.5507	3.1886	1.1972	–
M2C4N [12]	4.4591	18.0037	2.1523	–
Urea	5.66	6.304	0.781	7.3
KDP	7.28	7.394	7.90	8.93

prone to nucleophilic attack. Density overlap regions indicator Analysis and Hirshfeld analysis also supports that inter and intra-molecular interactions occur in morpholinium ring and tetrahedral ClO_4^- group. Electron distribution and reactivesites on the surface were analyzed using ELF and LOL. The predicted NLO properties of MP are much greater than those of urea and comparing some morpholinium derivative compounds. Consequently, MP crystal might be a good choice for high-speed optoelectronic applications.

CRediT authorship contribution statement

C.L. Shiny: Conceptualization, Data curation, Writing – original draft. **A. Arun Kumar:** Methodology. **C. Dabora Vincy:** Data curation. **X.D. Divya Dexlin:** Data curation. **J.D. Deephlin Tarika:** Data curation. **T. Joselin Beaula:** Supervision, Writing – review & editing.

Declaration of Competing Interest

The authors declare that they have no known competing financial interests or personal relationships that could have appeared to influence the work reported in this paper.

Data availability

The data that has been used is confidential.

Acknowledgement

The Author's thank Dr. I. Hubert Joe, Associate Professor in Department of Physics, Kerala University for granting us permission to do computational works in their Research Lab.

Supplementary materials

Supplementary material associated with this article can be found, in the online version, at doi:10.1016/j.molstruc.2023.135890.

References

[1] P. Szklarz, M. Owczarek, G. Bator, T. Lis, K. Gatner, K. Jakubas, Crystal structure, properties and phase transitions of morpholinium tetrafluoroborate [C4H10NO][BF4], J. Mol. Struct. 929 (1–3) (2009) 48–57, https://doi.org/10.1016/j.molstruc.2009.04.014.
[2] M. Galinski, I. Stepniak, Morpholinium-based ionic liquid mixtures as electrolytes in electrochemical double layer capacitors, J. Appl. Electrochem. 39 (2009) 1949–1953, https://doi.org/10.1007/s10800-009-9904-4.
[3] C. Brigouleix, M. Anouti, J. Jacquemin, M. Caillon-Caravanier, H. Galiano, D. Lemordant, Physicochemical characterization of morpholiniumcation based protic ionic liquids used as electrolytes, J. Phys. Chem. B 114 (2010) 1757–1766, https://doi.org/10.1021/jp906917v.
[4] R.N. Das, T.E. Sintra, J.A. Coutinho, S.P. Ventura, K. Roy, P.L. Popelier, Development of predictive QSAR models for Vibrio fischeri toxicity of ionic liquids and their true external and experimental validation tests, Toxicol. Res. 5 (2016) 1388–1399, https://doi.org/10.1039/c6tx00180g.
[5] M. Umadevi, V. Muthuraj, Molecular characterization, DFT and TD-DFT calculations of morpholinium tetra chloropalladate (II), J. Mol. Struct. 1138 (2017) 208–214, https://doi.org/10.1016/j.molstruc.2017.01.073.
[6] R. Bhuvaneswari, M. DivyaBharathi, G. Anbalagan, G. Chakkaravarthi, K. SakthiMurugesan, Molecular structure, vibrational spectroscopic (FT-IR, FT-Raman), NBO, HOMO and LUMO analysis of morpholinium oxalate by densityfunctional method, J. Mol. Struct. 1173 (2018) 188–195, https://doi.org/10.1016/j.molstruc.2018.06.109.
[7] R. Salmasi, A. Salimi, M. Gholizadeh, M. Rahmani, J.C. Garrison, Symmetric quaternary phosphoniumcation and perchlorate/chlorate anions: crystal structure, Database study and Hirshfeld surface analysis, J. Mol. Struct. 1179 (2019) 549–557, https://doi.org/10.1016/j.molstruc.2018.11.037.
[8] A. Arunkumar, P. Ramasamy, Studies on the structure, growth and characterization of morpholinium perchlorate single crystals, J. Crystal Growth 388 (2014) 124–131, https://doi.org/10.1016/j.jcrysgro.2013.10.005.
[9] V. Balachandran, G. Mahalakshmi, A. Lakshmi, A. Janaki, DFT, FT-Raman, FT-IR, HOMO-LUMO and NBO studies of 4-Methylmorpholine, Spectrochimica Acta Part A Molecular Biomolecular Spectros. 97 (2012) 1101–1110, https://doi.org/10.1016/j.saa.2012.07.112.
[10] J. George, M. George, J. Alex, D. Sajana, N.K. Shihab, G. Vinitha, R. Chitra, Growth of Morpholin-4-ium hydrogen tartrate single crystal for optical limiting application, Opt. Laser Technol. 119 (2019), 105647, https://doi.org/10.1016/j.optlastec.2019.105647.
[11] Ufuk Korkmaz, Yıldıray Topcu, Murat Tas, Ahmet Bulut, Synthesis, an experimental and quantum chemical computational study: proton sharing in 4-Morpholinium bis(hydrogen squarate), Spectrochim.Acta Part A Molecular Biomolecular Spectros. 134 (2015) 233–243, https://doi.org/10.1016/j.saa.2014.06.100.
[12] S. Karthick a, K. Thirupugalmani a, G. Shanmugam b, V. Kannan c, S. Brahadeeswaran, Experimental and quantum chemical studies on N-H…O hydrogen bonded helical chain type Morpholinium 2-chloro-4-nitrobenzoate: a phasematchable organic nonlinear optical material, J. Mol. Struct. 1156 (2018) 264–272, https://doi.org/10.1016/j.molstruc.2017.11.115.
[13] J.P. Perdew, Electronic Structure of Solids '91, Academic Verlag, Berlin, 1991. Ed. P. Ziesche and H. Eschrig,.
[14] M.J. Frisch, G.W. Trucks, H.B. Schlegel, G.E. Scuseria, M.A. Robb, J.R. Cheeseman, G. Scalmani, V. Barone, B. Mennucci, G.A. Petersson, H. Nakatsuji, M. Caricato, X. Li, H.P. Hratchian, A.F. Izmaylov, J. Bloino, G. Zheng, J.L. Sonnenberg, M. Hada, M. Ehara, K. Toyota, R. Fukuda, J. Hasegawa, M. Ishida, T. Nakajima, Y. Honda, O. Kitao, H. Nakai, T. Vreven, J.A. Montgomery Jr., J.E. Peralta, F. Ogliaro, M. Bearpark, J.J. Heyd, E. Brothers, K.N. Kudin, V.N. Staroverov, T. Keith, R. Kobayashi, J. Normand, K. Raghavachari, A. Rendell, J.C. Burant, S.S. Iyengar, J. Tomasi, M. Cossi, N. Rega, J.M. Millam, M. Klene, J.E. Knox, J.B. Cross, V. Bakken, C. Adamo, J. Jaramillo, R. Gomperts, R.E. Stratmann, O. Yazyev, A.J. Austin, R. Cammi, C. Pomelli, J.W. Ochterski, R.L. Martin, K. Morokuma, V.G. Zakrzewski, G. A. Voth, P. Salvador, J.J. Dannenberg, S. Dapprich, A.D. Daniels, O. Farkas, J.B. Foresman, J.V. Ortiz, J. Cioslowski, D.J. Fox, Gaussian 09, Revision C.02, Gaussian Inc., Wallingford CT, 2010.

[15] E.D. Glendening, J.K. Badenhoop, A.E. Reed, J.E. Carpenter, J.A. Bohmann, C. M. Morales, F. Weinhold, NBO 3.1, Theoretical Chemistry Institute, University of Wisconsin, Madison, 2001.
[16] T. Sundius, Scaling of ab Initio Force Fields by MOLVIB, Vib. Spectrosc. 29 (2002) 89–95. http://doi.org/10.1016/S0924-2031(01)00189-8.
[17] T. Sundius, Molvib-A Flexible Program for Force Field Calculations, J. Mol. Struct. 218 (1990) 321–326. http://doi.org/10.1016/0022-2860(90)80287-T.
[18] S.K. Wolff, D.J. Grimwood, J.J. McKinnon, M.J. Turner, D. Jayatilaka, M. A. Spackman, Crystal Explorer (Version 2.2), University of Western Australia, Crawley, Australia, 2010.
[19] T. Lu, F. Chen, Multiwfn: a multifunctional wavefunction analyser, J. Comput. Chem. 33 (2012) 580–592, https://doi.org/10.1002/jcc.22885.
[20] W. Humphrey, A. Dalke, K. Schulten, VMD: visual molecular dynamics, J. Mol. Graph. 14 (1996) 33–38. 10.1016/0263-7855(96)00018-5.
[21] Computational Chemistry Comparison and Benchmark Data Base Release 21 August 2020. NIST Stand. Ref. Database 101.
[22] T. Joselin Beaula, A. Packiavathi, D. Manimaran, I. Hubert Joe, V.K. Rastogi, V. BenaJothy, Quantum chemical computations, vibrational spectroscopic analysis and antimicrobial studies of 2,3-Pyrazinedicarboxylic acid, Spectrochim. Acta Part A: Molecular Biomolecular Spectros. 138 (2015) 723–735, https://doi.org/10.1016/j.saa.2014.11.034.
[23] F.H. Allen, O. Kennard, D.G. Watson, L. Brammer, A.G. Orpen, Tables of bond lengths determined by X-Ray and neutron diffraction. Part 1. Bond lengths in organic compounds, J. Chem. Soc. Perkin Trans. II (1987) S1–S19, https://doi.org/10.1039/P298700000S1.
[24] R.J. Gillespie, the VSEPR model revisited, Chem. Soc. Rev. 59 (1992) 59–69, https://doi.org/10.1039/CS9922100059.
[25] D. Manimaran, C. Jesintha John, V.K. Rastogi, I. Hubert Joe, Growth and vibrational spectral investigation of nonlinear optical crystal L-Argininum perchlorate-DFT study, Spectrochim. Acta Part A Molecular Biomol. Spectros. 109 (2013) 173–178, https://doi.org/10.1016/j.saa.2013.02.024.
[26] F.R. Dollish, W.G. Fateley, F.F. Bentley, Characteristic Raman Frequencies of Organic Compounds, Wiley, NewYork, 1973.
[27] Gyorgy Varsanyi, L. Lang, Assignment For Vibrational Spectra of Seven Hundred Benzene Derivatives, Wiley & Sons, New York, 1974.
[28] K. Venkateswaran, M. Karnan, R. Muthukumar, Experimental and Theoretical DFT studies on vibrational spectra and Molecular docking studies of 4-(Chloroacetyl) Morpholine, J. Inf. Comput. Sci. 9 (8) (2019). ISSN: 1548-7741, http://www.joics.org/ics-1310.
[29] S. Kumar, A.K. Rai, S.B. Rai, D.K. Rai, Infrared and Raman spectra of Histidine: anab initio DFT calculations of Histidine molecule and its different protonated forms, Ind. J. Phys. 84 (2010) 563–573, https://doi.org/10.1007/s12648-010-0039-6.
[30] S. Gunesekaran, R. Thilak Kumar, S. Ponnusamy, Vibrational spectra and normal coordinate analysis of diazepam, phenytoin and phenobarbitone' Spectrochim, Acta, Part A 65 (2006) 1041, https://doi.org/10.1016/j.saa.2006.01.037.
[31] R.M. Silverstein, G.C. Bassler, T.C. Morrill, Spectrometric Identification of Organic Compounds, 3rd ed., John Wiley & Sons, New York, NY, 1974, p. 239, https://doi.org/10.1021/ed039p546.
[32] J.W. Nebgen, A.D. McElroy, H.F. Klodowski, Raman and infrared spectra of nitronium perchlorate, Inorg. Chem. 4 (1965) 1796–1799, https://doi.org/10.1021/ic50034a030.
[33] Smita S. Patil, Samina K. Tadavi, Amol Dikundwar, Ratnamala S. Bendre, The transition metal complexes of Fe(II), Ni(II) and Cu(II) derived from phthalazine based ligands: synthesis, crystal structures and biological activities, J. Mol. Struct. 1247 (2022), 131293, https://doi.org/10.1016/j.molstruc.2021.131293.
[34] A.T. Maynard, M. Huang, W.G. Rice, D.G. Covell, Reactivity of the HIV-1 nucleocapsid protein p7 zinc finger domains from the perspective of density-functional theory Proc, Natl. Acad. Sci. USA. 95 (20) (1998) 11578–11583, https://doi.org/10.1073/pnas.95.20.11578.
[35] R.G. Parr, W. Yang, The Kohn-Sham method: basic principles. Density-Functional Theory of Atoms and Molecules, Oxford University Press, New York, 1989, pp. 142–168.
[36] Bryan M. Wong, Timothy H. Hsieh, Optoelectronic and excitonic properties of oligoacenes: substantial improvements from range-separated time-dependent density functional theory, J. Chem. Theory Comput. 6 (2010) 3704–3712.
[37] A.E. Raeber, B.M. Wong, The importance of short- and long-range exchange on various excited state properties of DNA monomers, stacked complexes, and Watson-Crick pairs, J. Chem. Theory Comput. (2015). http://pubs.acs.org.
[38] G. Parr, P.K. Chattaraj, Principle of maximum hardness, J. Am. Chem. Soc. 113 (5) (1991) 1854–1855, https://doi.org/10.1021/ja00005a072.
[39] R.G. Parr, L.V. Szentpaly, S. Liu, Electrophilicity index, J. Am. Chem. Soc. 121 (9) (1999) 1922–1924, https://doi.org/10.1021/ja983494x.
[40] M. Chen, U.V. Waghmare, C.M. Friend, E. Kaxiras, A density functional study of clean and hydrogen-covered α-MoO3 (010): α-MoO3 (010): electronic structure and surface relaxation, J. Chem. Phys. 09 (1998) 145–154, https://doi.org/10.1063/1.477252.
[41] Saswata Halder, Ram Awdhesh Kumar, Ritwik Maity, T.P. Sinha, A tailored direct-to-indirect band structure transition in double perovskite oxides influences its photocatalysis efficiency, Ceram. Int. 49 (5) (2023) 8634–8645.
[42] Peverga R. Jubu, O.S. Obaseki, A. Nathan-Abutu, F.K. Yam, Yushamdan Yusof, M. B. Ochang, Dispensability of the conventional Tauc's plot for accurate bandgap determination from UV-vis optical diffuse reflectance data, Results Opt. 9 (2022), 100273, https://doi.org/10.1016/j.rio.2022.100273.
[43] F.L. Hirshfeld, Bonded-atom fragments for describing molecular charge densities, Theor. Chim. Acta 44 (1977) 129–138. 10.1007/BF00549096.
[44] M.A. Spackman, J.J. McKinnon, Fingerprinting intermolecular interactions in molecular crystals, Cryst. Eng. Comm. 4 (66) (2002) 378–392, https://doi.org/10.1039/b203191b.
[45] S. Christopher Jeyaseelan, A. Milton Franklin Benial, Quantum chemical, spectroscopic investigations, molecular docking and cytotoxic evaluation of 1-Methyl-indole-3-carboxaldehyde, Chem. Data Collect. 33 (2021), 100698, https://doi.org/10.1016/j.cdc.2021.100698.
[46] B. Fathima Rizwana, J.C. Prasana, S. Muthu, C.S. Abrahama, Molecular docking studies, charge transfer excitation and wave function analyses (ESP, ELF, LOL) on valacyclovir : a potential antiviral drug, Comput. Biol. Chem. 78 (2019) 9–17, https://doi.org/10.1016/j.compbiolchem.2018.11.014.
[47] P. De Silva, C. Corminboeuf, Simultaneous visualization of covalent and non covalent interactions using regions of density overlap, J. Chem. Theory Comput. 10 (2014) 3745–3756, https://doi.org/10.1021/ct500490b.
[48] M.A.M. El-Mansy, A. Suvitha, W. Osman, K.F. Khaled, Exploring the electronic and optical absorption properties for homo- and Hetero-Pyrrole-Graphene quantum dots, J. Comput. Electron. 20 (6) (2021) 2387, https://doi.org/10.1007/s10825-021-01773-w.